How Gaseous Environment Influences a Carbon Nanotube-based Mechanical Resonator

Yihan Nie[1], Haifei Zhan[1],, Zhuoqun Zheng[1, 2], Arixin Bo[1], Edmund Pickering[1], and Yuantong Gu[1,*]*

[1]School of Chemistry, Physics and Mechanical Engineering, Queensland University of Technology (QUT), Brisbane QLD 4001, Australia

[2]College of Mathematics, Jilin University, 2699 Qianjin Street, Changchun, 130012, China

ABSTRACT

Nanoscale mechanical resonator-based nanoelectromechanical systems (NEMS) have been reported with ultra-high sensitivity, which are normally acquired from an ultra-vacuum environment at cryostat temperature. To facilitate their practical applications for gas sensing or bio-detection, it is critical to understand how the fluid (gas or liquid) environment will impact the resonance behaviours of the nano-resonator. This work reports a first-time comprehensive investigation on the influence of the N_2 gaseous environment on the resonance properties of carbon nanotube (CNT)-based mechanical resonator, through a combination of grand canonical Monte Carlo and large-scale molecular dynamics simulations. It is shown that the gaseous environment exerts a significant effect on the resonance properties of the CNT resonator through a dynamic desorption and re-adsorption process. Under the temperature of 100 K and the pressure of 1 bar, the displacement amplitude of the CNT resonator is found to experience a sharp reduction of about 82% within first 90 ps vibration in the N_2 gaseous environment. Further, a large initial excitation is found to result in smaller adsorption and a reduced damping effect. For instance, when the excitation amplitude increases from 2 Å/ps to 8 Å/ps, the damping ratio receives more than 40% reduction. It is found that higher pressure leads to a smaller resonance frequency and enhanced damping effect, while higher temperature induces an increase in the resonance frequency but a decrease in the damping ratio. This work shows that the gaseous environment has a marked impact on the vibrational properties of nano-resonators, which should shed lights on the applications of mechanical nano-resonators in fluid environment.

Introduction

Nanoscale mechanical resonator-based nanoelectromechanical systems (NEMS) have drawn significant interests from both scientific and engineering communities in the past decade due to their extraordinary sensitivity. A large variety of emerging NEMS applications have been developed in areas such as mass spectrometry (reaching a single-proton level),[1-3] force spectrometry[4-5] (such as single-molecule force[6]), ultrasound vibrations detection (for subsurface characterization),[7] insulating electronic states measurement.[8] The excellent NEMS sensitivity is enabled through a combination of ultra-small mass, stiffness, and precise resonant frequency *f* determination in the nano-resonator, which allows perturbations to that frequency δf (such as mass or force) to be detected.[9] Different low-dimensional nanomaterials have been utilized to construct nanoscale mechanical resonators, including nanoparticles,[10] one-dimensional (e.g., CNT[11] or nanowire[12]) and two-dimensional (e.g., graphene[13] and MoS_2[13]) nanomaterials. In theory,[14-15] the mass sensitivity for the NEMS can be calculated from $\langle \delta f/f \rangle \sim 10^{-DR/20}/2Q$. Here, *DR* is the dynamic range (in the unit of dB), which is the power level associated with the signal-to-noise ratio (*SNR*). *Q* is the quality factor, which is a measure of the energy dissipation per vibration cycle (through internal or external loss channels).[16] In this regard, there are extensive efforts being devoted to achieve a high *Q* for better resolution.[10, 17-18]

To date, majority of the reported high sensitivity was measured from a vacuum condition at a cryostat temperature.[19] However, a number of applications require the mechanical nano-resonator operating in a fluid (i.e., a gas or a liquid), such as the application in biological detection,[20-22] gas sensing,[23] chemical vapor sensing,[24-28] or atmospheric pressure sensing.[9] Therefore, it is crucial to understand how the nanoresonators would behave in a gaseous environment. However, the influence from the fluid environment at nanoscale is still widely unexplored. The viscous drag by the fluid medium is expected to induce significant

impact on the Q of the resonator. In addition to that, there are extensive experimental measurements[29] and simulation results[16] showing a marked reduction of Q at higher temperature. As such, to maintain a high sensitivity for practical applications in fluid environment at a certain temperature (e.g., ambient temperature) becomes crucial for the NEMS. Earlier experiments have shown a low Q of around 40 for CNT-based resonator even at a pressure less than 1 Torr (at room temperature), which decreases when the pressure increases.[30] In comparison, later experiments reported a Q up to 5 million in ultra-clean condition at a temperature of 30 mK.[19] Such significant change of the Q signifies the profound impacts on the sensitivity of NEMS from the fluid (liquid or gaseous) environment.

Plenty of works have investigated the resonant or vibrational behaviours of micro-scale resonators in fluid environment.[31-32] However, how the fluid environment impact the resonant behaviour at nanoscale is still largely lacking. Besides the free gas molecules in the environment, the adsorbed ones are expected to exert significant influence on the vibrational properties of the resonator at nanoscale. Extensive studies have shown a significant gas adsorption on nanomaterials or nanostructure due to their large surface-to-volume-ratio,[33] through grand canonical Monte Carlo (GCMC) method[34-35] and density function theory (DFT) calculations.[36] To this end, this work aims to explore how the gas environment introduces adsorption, and alters the resonance behaviour of CNT-based mechanical resonator. Based on a serial of *in silico* studies considering a representative N_2 gaseous environment, this work establishes a first time understanding of the coupled effects from the gaseous environment and finite temperature on the resonance frequency and damping ratio (or Q factor) of the CNT-based mechanical resonator.

Methods

Model Establishment. The grand canonical Monte Carlo (GCMC) method was employed to simulate the gas adsorption on the CNT both inside and outside the tube under different pressure and temperature [37], which describes the system in the grand canonical (μVT) ensemble (where the chemical potential μ, volume V, and temperature T are constants). The single-wall open end CNT (10,10) was considered as the adsorbent (with a length of 173.24 Å), and N_2 was the adsorbate. N_2 can be adsorbed on both internal and external surface of (10, 10) CNT.[38] To mimic the adsorption of the open end CNT, GCMC moves are performed in the internal region and external region of the CNT.[39] The commonly used adaptive intermolecular reactive empirical bond order (AIREBO) potential was employed to describe the C-C atomic interactions within the CNT.[40] This potential has been shown to well represent the binding energy and elastic properties of carbon materials. The N-N atomic interactions were described by a harmonic potential, given by $E_{bond} = K(r - r_0)^2$, where $r_0 = 1.1$ Å is the equilibrium bond length, and $K = 71.6\ eV/\text{Å}^2$ is the bond coefficient. The atomic interactions between C and N were described by the 12-6 Lennard-Jones (LJ) potential $\phi_{ij} = 4\varepsilon[(\sigma/r_{ij})^{12} - (\sigma/r_{ij})^6]$, where $\varepsilon = 2.88\ meV$, and $\sigma = 3.36$ Å.[35] The cut-off distance of LJ potential was chosen as 10 Å. A periodic cuboid simulation box (a size of 5.41×5.41×21.32 nm^3) was considered, where CNT was located in the middle. The chemical potential of gas reservoir was calculated as ideal gas. During the GCMC process, gas molecules were inserted or deleted for 2×10^6 times, and the system finally reached an equilibrium status for chemical potential (with the total gas molecule number saturated to a certain value). After the equilibrium, another GCMC process was conducted to avoid the error of tail corrections caused by the increase of the system density for 1×10^5 time steps. The gas molecules were fixed rigid during GCMC simulation, i.e., no intra-molecular interactions. The final adsorption model was further equilibrated by a heating and annealing process using molecular dynamics (MD) simulations

to assess the stability of the model. All simulations were performed with Large-scale Atomic/Molecular Massively Parallel Simulator (LAMMPS).[41]

Vibration Simulation. Based on the equilibrated adsorption model established from the GCMC simulation, the vibration simulation was carried out by fixing two ends of the CNT (mimicking a doubly-clamped configuration). A further relaxation under a canonical (NVT) ensemble of the system was performed (for 250 ps). Nose-Hoover thermostat is adopted to maintain the temperature.[42] Thereafter, a transverse velocity excitation was applied to the CNT, which has a distribution of sine function along the CNT axis, i.e. $v_x(z) = \lambda sin\ (kz)$.[43-45] Without further declaration, the velocity excitation was applied to both the CNT and its internal and external gas adsorbates, and the magnitude λ was set to 1 Å/ps. The vibration simulation was conducted under a microcanonical (NVE) ensemble (where the number of atoms N, the system volume V, and the total energy E are constants). Periodic boundary conditions were kept during the vibration simulation to mimic an infinite open space. A small time step of 0.5 fs was used for all simulations.

Results and Discussion

Resonance Characteristics. **Figure 1a** shows the front view of the configuration of the CNT after N_2 adsorption at the temperature of 100 K and a pressure of 0.5 bar. Due to its open ends and relatively large diameter compared with the size of the individual N_2 molecule, N_2 molecules can enter into CNT and be adsorbed on the CNT internal surface, as well as the external surface (Figure 1b). The adsorption amount follows the classic Langmuir theory in the investigated pressure range (see **Supporting Information S1**). The adsorption amount used for vibration test can be found in **Supporting Information S2**. Since no charge is considered in the system, the only interactions between CNT and N_2 molecules are van der Waals (vdW)

interactions, which causes adsorption, and increases the low frequency phonon density of state in N_2 (see **Supporting Information S3**). It is worthy to mention that wider CNTs are utilized in experiments to construct the mechanical resonators, which will induce more internal adsorption and thus result in stronger effect on their resonators properties.

According to the adsorption configuration, the gaseous environment may influence the resonators through free gas molecules and adsorbates (either on internal or external surfaces). In reality, the internal adsorbates only exist in open end CNTs, and the closed end prevents the CNT from the internal adsorption.[46] Thus, four different vibration scenarios are simulated for CNT resonators fabricated by different processes, including: S1 - vibration in a vacuum condition; S2 - vibration in a complete gaseous environment (with full adsorption and free gas molecules, mimics an open end CNT resonator in reality); S3 - vibration in a vacuum condition with only internal adsorption (mimics an open end CNT resonator manufactured in gaseous environment, but work in vacuum with two end sealed); and S4 - vibration with only external adsorption and free gas molecules (mimics an closed end CNT). The partial adsorption models are obtained by removing the irrelevant gas molecules after GCMC simulations. According to the radial distribution function (RDF, see **Supporting Information S4**), part of the internal N2 adsorption is in a liquid-like phase at low temperature. A velocity excitation is applied to the system in the transverse direction (x-axis in Figure 1) to activate the vibration of the CNT, which has a distribution of sine function along axis, i.e. $v_x(z) = \lambda sin\,(kz)$.[43] The velocity excitation is applied to both the CNT and its internal and external gas adsorbates. The adsorption model at 100 K and a pressure of 0.5 bar are used for vibration simulations unless otherwise specified.

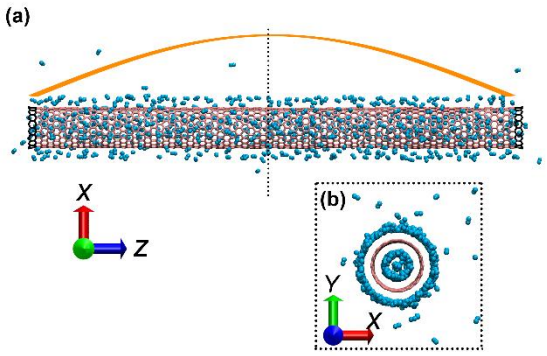

Figure 1. A segment of the (10, 10) CNT with N_2 gas adsorption on both internal and external surfaces (at 100 K, 0.5 bar). Upper panel (a) is the front view and the bottom panel (b) is the cross-sectional view.

Figure 2 compares the time trajectory of the displacement of the CNT mass centre recorded from these four types of vibration simulations. Due to the intrinsic friction and clamped boundary conditions, the pristine CNT experiences a slight damping during the vibration (S1, Figure 2a).[47] Compared to the vibration in the vacuum condition, a significant damping effect is observed for the vibration in the complete gaseous environment (S2, Figure 2b). For instance, the displacement amplitude is found to experience a sharp reduction of about 82% within first 90 ps vibration (from 1.5 Å to 0.27 Å). In particular, after the initial sharp reduction, the displacement of the mass centre along the excited direction can hardly be resolved from the noise (with a magnitude around 0. 25 Å). In comparison, a gradual reduction of the displacement amplitude is observed for the CNT with only internal adsorption (S3, Figure 2c), and the displacement amplitude receives ~ 78% reduction after 1000 ps vibration. Different results are observed for the vibration with external gas (S4, Figure 2d), from which a significant reduction of the displacement amplitude is detected within the first 100 ps vibration. These results signify that the free gas molecules together with the external adsorption induces a remarkable damping effect to the vibrational behaviour of the CNT. Overall, the gaseous

environment (coupled with the gas adsorption) exerts a significant damping effect to the CNT mechanical resonator.

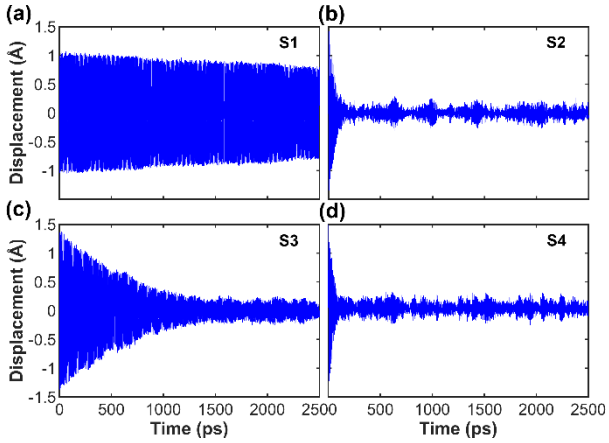

Figure 2. The time history of the displacement of the CNT mass centre for the vibration under a temperature of 100 K and a pressure of 0.5 bar. (a) Vibration in a vacuum condition – S1; (b) Vibration in a complete N_2 atmosphere with full adsorption – S2; (c) Vibration with only internal adsorption – S3; and (d) Vibration with external adsorption and free gas molecules – S4.

Based on the time history of the displacement of the CNT mass centre, we apply the fast Fourier transformation (FFT) to extract the resonance natural frequencies. For the vibration in the vacuum condition (S1), a clean frequency spectrum is resolved, which shows a natural frequency of around 141.73 GHz (**Figure 3**a). According to the continuum mechanics, the frequency of the undamped CNT can be estimated from $\omega_n = \frac{{\beta_n}^2}{2L^2}\sqrt{Y(a^2+b^2)/\rho}$, where a and b are the inner and outer radius, respectively; L and ρ are the length and density, respectively; β_n is a constant determined by the boundary condition, and Y is Young's modulus. In this regard, Young's modulus of the CNT(10,10) is estimated as 1.26 TPa, which agrees well with previous experimental work.[48] Similar with the resonance under a vacuum condition, a similar clean frequency spectrum but smaller value (~ 129.97 GHz) is derived for the vibration with only internal adsorption (S3, Figure 3b). In comparison, the frequency spectrum

suffers from significant noise when the CNT vibrates with external adsorption and free gas molecules, either with (S2) or without internal adsorption (S4) (Figure 3c and 3d). Such noise can be decomposed into the white noise, and the frequency fluctuation.[49] The white noise is caused by the uncorrelated frequencies in the system, which has the same amplitude in all frequency range.[50] The frequency fluctuation is the shift of frequency response, which has a larger amplitude around the natural frequency. Theoretically, the adsorption and desorption of the gas molecules, and the diffusion of adsorbed gas molecules can change the frequency response of the CNT resonator, causing the frequency fluctuation.[51-52] To evaluate the noise brought by gas molecules, we calculate the Allan variance σ_A to further analysis the frequency spectrum components, which is estimated according to[49]

$$\sigma_A^2(\tau_A) = \frac{1}{2f_c^2}\frac{1}{N-1}\sum_{m=2}^{N}(\bar{f}_m - \bar{f}_{m-1})^2 \quad (1)$$

The calculation divides the whole signal into *N* intervals in time domain, with τ_A as the time interval length (in the unit of ps) and f_c as the average frequency in the whole time domain. $\bar{f}_m$ is the average frequency in the *m*th interval. With the increase of τ_A, the Allan variance decreases if the noise is the white noise; it retains as a constant when there is only frequency fluctuation; for the combination of both, the Allan variance will decrease and converge to the value determined by frequency fluctuation. For all the tested τ_A, the Allan variance decreases continuously with the time interval length in the full or partial gaseous environment (S2, S3, S4, see Figure 3e and 3f), indicating the profound influence on the resonance behaviours of the CNT resonator from the white noise. A converged Allan variance is not observed (Figure 3e and 3f), which is due to the insufficient simulation time. Refer to the experimental measurements for the Si nanoresonators, the Allan variance saturates when the time interval is longer than 1 s.[49] A significantly longer simulation time is required to further analyse the Allan variance (up to 10^9 times longer if considering 1 s time interval), which exceeds our current computational capacity and beyond the scope of the current work.

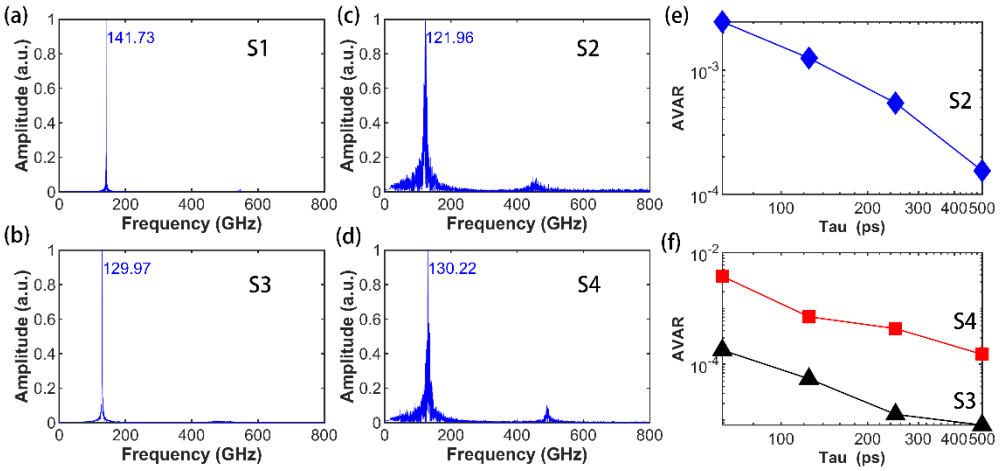

Figure 3. Natural frequency spectrum of the CNT resonator. (a) Vibration in a vacuum condition - S1; (b) Vibration in a vacuum condition with only internal adsorption - S3; (c) Vibration in a complete N_2 atmosphere with full adsorption - S2; (d) Vibration with external gas - S4. (e) The Allan variance as a function of the time interval for the vibration scenario of: (e) S2, and (f) S3 and S4.

To affirm above observations, we perform a serial of simulations by varying the vibration settings (based on the same full adsorption model at the temperature of 100 K and the pressure of 0.5 bar). First, considering that the adsorbed gas molecules are randomly distributed on the CNT surfaces, we perform the resonance tests in four transverse directions, i.e., imposing the vibration excitation along *x, z, x=z,* and *x=-z* directions (refer to the model in Figure 1a). Second, we alter the excitation approach by adding the excitation only to the CNT and the internal adsorption. All of these tests yield to similar results, i.e., a sharp reduction (~ 80%) of the displacement of the mass centre within a simulation time of about 100 ps, which fluctuates around 0.25 Å afterwards (see **Supporting Information S5** for full results).

Dynamic adsorption-desorption process. To unveil how the gaseous environment affect the vibrational behaviour of the CNT resonator, we assess the atomic configurations of the system during vibration. **Figure 4**a compares the time history of the displacement of the CNT mass

centre and the total N_2 adsorption during vibration with a small excitation velocity (1 Å/ps). It is found that the total adsorption amount fluctuates around a certain value, indicating a stable adsorption during the vibration. Figure 4b and 4c illustrate the trajectory of a randomly picked gas molecule absorbed on the internal and external CNT surface during a simulation time of 250 ps. While the movement of the internal or external gas molecules is constrained inside or outside the CNT, they exhibit a large relative movement along the CNT surfaces. Figure 4d compares the atomic configurations of the system at different status, including the initial stats, at a maximum displacement, and after 1000 ps vibration. As is seen, the configuration is nearly unchanged.

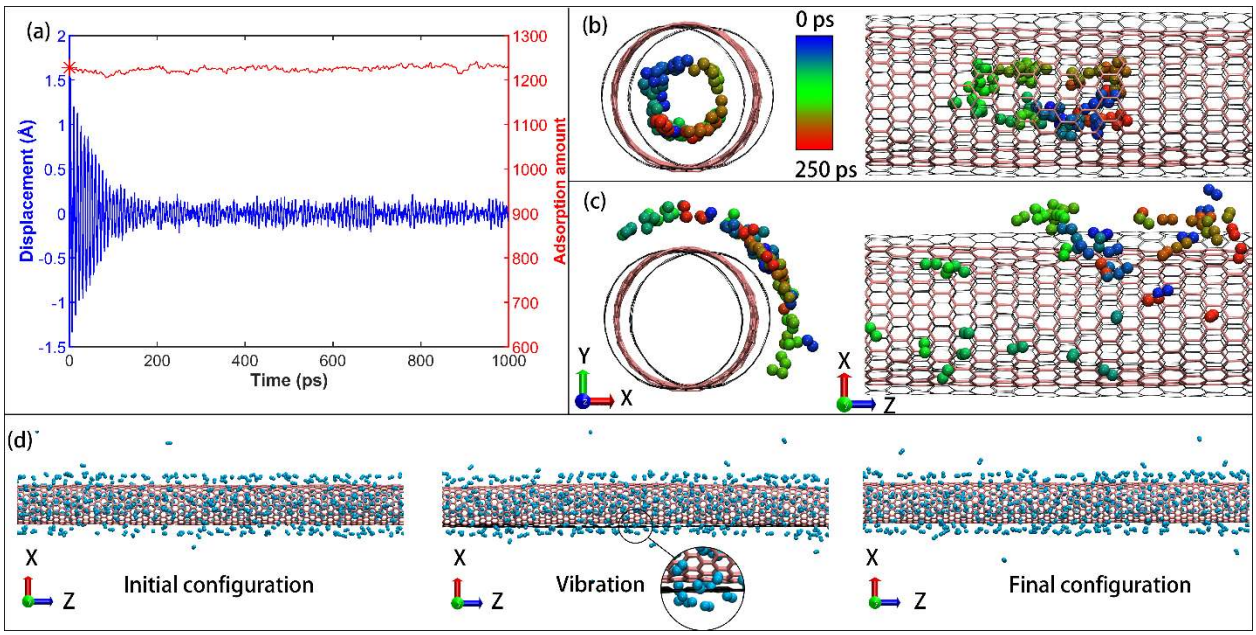

Figure 4. Gas adsorption during the vibration of the CNT with an excitation amplitude of λ=1 Å/ps. (a) The time history of the displacement of the CNT mass centre and the total adsorption amount. The red star marker highlights the initial adsorption amount. The trajectories of a randomly picked N_2 molecule adsorbed on: (b) the internal surface, and (c) the external surface of the CNT during the vibration. Left panel is the cross-sectional view, and right panel is the front view. The black circles in the left panel represent the maximum displacement during vibration. The trajectories are coloured according to the simulation time with an interval of 250

ps. (d) The atomic configurations of the system before vibration (left panel), at a maximum displacement (middle panel), and after 1000 ps vibration (right panel).

To further assess the influence from the gas adsorption, we consider the vibration of the CNT mechanical resonator under a larger displacement of the mass centre. For such purpose, we increase the initial excitation amplitude λ from 0.6 Å/ps from 8 Å/ps. It is found the increase of the excitation will induce a significant occurrence of the adsorption-desorption of the N_2 molecules during the vibration. As illustrated in **Figure 5**a, there are three distinguishable changing stages of the adsorption amount for the vibration under an excitation velocity of 8 Å/ps. Due to the sudden large velocity excitation, a strong desorption is observed at the beginning of the vibration, and the total adsorption amount is reduced sharply from 1200 to 650 (within 50 ps, stage I - desorption). Thereafter, the total adsorption amount recovers to around 790 (stage II – re-adsorption), and fluctuates around this value with continuing vibration (corresponding to around 37% of the initial adsorption amount, state III – saturated adsorption). As aforementioned, the N_2 molecules are attached to the CNT surfaces through weak vdW interactions, i.e., physisorption. It is assumed that under higher excitation velocity, the physisorption strength is not strong enough to provide the adsorbed gas molecules sufficient acceleration/deceleration to follow the movement of the CNT. As such, they are "shaken off" from the CNT surfaces, resulting in a desorption process. Such desorption phenomenon is well reflected in the atomic configurations in Figure 5b and 5c, from which the trajectories of a randomly picked gas molecule absorbed on the internal and extern surfaces do not follow the vibration of the CNT. After 1000 ps vibration, the amount of the free gas molecules increases significantly compared to the initial configuration (Figure 5d). The desorption is a direct signature of the damping effect that coverts the kinetic energy into the thermal energy of the system, i.e., increase the temperature. As is well understood, the adsorption amount decreases when the temperature rises, which is in line with the reduced adsorption amount after damping.

For the vibration with a small excitation, the temperature rise is not obvious and thus the adsorption amount remains nearly a constant. A detailed temperature increment for the adsorbed N_2 and free N_2 molecules after damping is compared in the **Supporting Information S6**. Besides the overall temperature increment, we also calculated the kinetic energy of the N_2 molecules corresponding to their translational, rotational, and vibrational degree of freedoms, from which, an overall increase of these kinetic energy components are observed after the damping process (see details in **Supporting Information S7**).

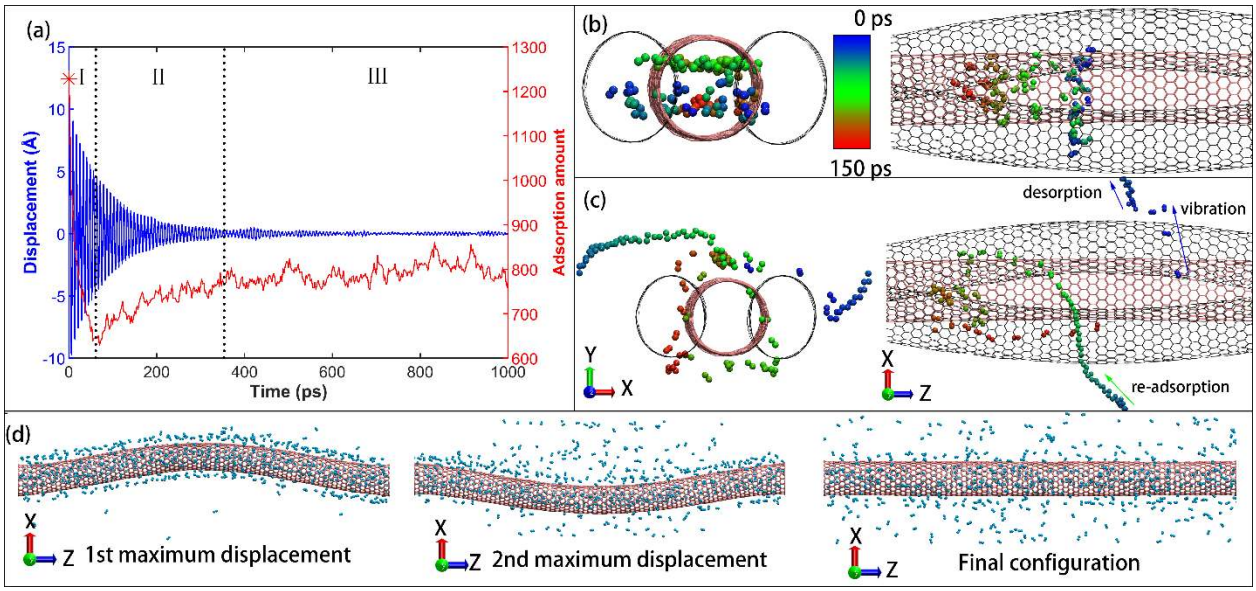

Figure 5. Gas adsorption during the vibration of the CNT with an excitation amplitude of λ=8 Å/ps. (a) The time history of the displacement of the CNT mass centre and the total adsorption amount. The red start marker highlights the initial adsorption amount. The trajectories of a randomly picked N_2 molecule adsorbed on: (b) the internal surface of the CNT, and (c) the external surface of the CNT during the vibration. Left panel is the cross-sectional view, and right panel is the front view. The black circles in the left panel represent the maximum displacement during vibration. The trajectories are coloured according to the simulation time with an interval of 150 ps. (d) The atomic configurations of the system before vibration (left panel), at a maximum displacement (middle panel), and after 1000 ps vibration (right panel).

Figure 6a compares the maximum displacement amplitude (Δd_m, acquired from the first vibration cycle), the instantaneous adsorption loss ratio, and the equilibrium adsorption loss ratio under the excitation magnitude λ ranging from 0.6 Å/ps to 8 Å/ps. Here, the instantaneous adsorption loss ratio is defined as $\eta_{in} = (n_0 - n_{min})/n_0$, where n_0 is the initial adsorption amount before vibration, and n_{min} is the adsorption amount after desorption at the end of the initial desorption - stage I. The equilibrium adsorption loss ratio is defined as $\eta_{eq} = (n_0 - n_{ave})/n_0$, with n_{ave} as the adsorption amount averaged over 500 ps simulation time during the equilibrium vibration stage (i.e., from 2000 ps to 2500 ps). Basically, the maximum displacement amplitude (Δd_m) has a good linear relationship with the excitation magnitude λ, especially at smaller excitation magnitude range. Simplifying the CNT resonator as a mass-spring system, the potential energy stored in the system during the resonance can be calculated by $k\Delta d_m^2/2$ in the linear regime, and the excitation (kinetic) energy as imposed on the system equals to $m\bar{\lambda}^2/2$. Thus, a good linear relationship between Δd_m and $\bar{\lambda}$ indicates that the CNT resonator is vibrating essentially in the linear regime. Here k and m are the equivalent spring constant and mass, and $\bar{\lambda}$ is the equivalent initial excitation velocity. Along with the increase of the velocity excitation, a continuously increasing instantaneous desorption ratio and equilibrium loss ratio continuously is observed. That is, larger initial excitation induces stronger initial desorption and leads to less adsorption amount after equilibrium.

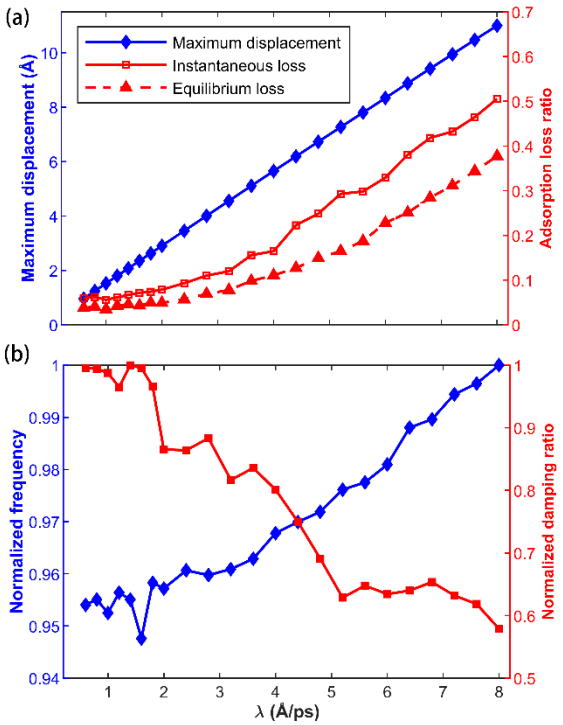

Figure 6. Vibrational properties under varies excitation magnitudes. (a) The maximum displacement amplitude Δd_m, the instantaneous adsorption loss ratio η_{in}, and the equilibrium adsorption loss ratio η_{eq} as a function of the excitation magnitude; and (b) The normalized resonance frequency and damping ratio as a function of the excitation magnitude.

The initial excitation not only affects the gas adsorption, but also influences the resonance frequency and the damping ratio as shown in Figure 6b. The damping ratio ζ is estimated using logarithmic decrement (LDM) method based on the recorded time history of the displacement,[53]

$$\frac{A_{i+r}}{A_i} = \exp\left[-\frac{\zeta}{\sqrt{1-\zeta^2}} 2\pi n\right] \tag{2}$$

Here, A_i represents the displacement amplitude in the ith vibration cycle, and n is the total vibration cycle. Both damping ratio and resonance frequency are averaged from four simulations (with velocity excitations being imposed in four different directions) and normalized in relative to their maximum value. In general, the damping ratio is found to experience a marked decrease when the excitation amplitude increases, e.g., the damping ratio

reduces more than 40% when the excitation amplitude increases from 2 Å/ps to 8 Å/ps. Since the amount of free gas molecules increases with severe desorption (at higher excitation amplitude), the decreasing damping ratio implies that the damping effect is dominated by the adsorbed gas molecules, rather than the free gas molecules. In comparison, the resonance frequency of the CNT increases slightly with the excitation amplitude increase (less than 5%). Such increasing tendency can be explained from two perspectives. First, considering the CNT resonator as a mass-spring system, its natural frequency is determined by the mass and equivalent spring constant, i.e., $f = \sqrt{k/m}\,/2\pi$. Since larger excitation leads to smaller adsorption, which will thus reduce the mass and yields to a larger frequency (here the gas adsorption is assumed to have negligible effect on the equivalent spring constant). Second, for the doubly clamped CNT resonator, the increasing excitation amplitude will lead to severer axial extension during vibration, which will increase the extracted resonance frequency.[54]

Thermal influence. Considering the strong correlation between the gas adsorption and the temperature, it is critical to probe how the gas environment would affect the vibrational behaviours of the CNT resonator at different temperatures. In this regard, a serial of GCMC simulations are conducted to establish the CNT resonator system with gas adsorption under the temperature ranging from 100 K to 400 K (with the pressure of 1 bar). A small excitation magnitude of 1 Å/ps is adopted to minimize the temperature increase induced by the added velocity excitation. For comparison purpose, the vibrations of the CNT resonator under a vacuum condition are also revisited. The simulation models under different temperatures are established from the GCMC simulations. As expected, both internal and external adsorption amount decreases continuously with temperature (see Supporting Information S2). According to the equation of status for ideal gas (i.e., $PV = NRT$), there are around 15 free N_2 molecules in the simulation domain if the adsorption phenomenon is ignored (at 300 K and 1 bar). Here, P, V and N represent the pressure, volume, and the number of gas molecules. R is the gas

constant, and *T* is the temperature. That is, the adsorption phenomenon is non-ignorable even at ambient temperature.

Figure 7a compares the resonance frequency of the CNT resonator as a function of temperature. For the scenario under a vacuum condition (S1), the frequency is nearly a constant (fluctuating around 142 GHz), indicating an ignorable influence of the temperature on pure CNT vibration. In comparison, the resonance frequency increases when the temperature increases under either a partial/full gaseous environment (S2, S3 and S4). Such observation is reasonable as the corresponding initial model has less adsorption amount at higher temperature. Refer to the mass-spring approximation, the resonance frequency (*f*) of the CNT with gas adsorption can be calculated from

$$f = f_0\sqrt{\frac{m_0}{m_0+\Delta \mathrm{m}}} \tag{3}$$

Here, f_0 is the natural frequency without adsorption, m_0 is the mass of the CNT, and Δm is the adsorption mass. Thus, the reduced adsorption amount (at higher temperature) will lead to an increase in the resonance frequency. To note that, the frequency shift (Δf) in a mechanical resonator is commonly calculated from $\Delta f = -\frac{\Delta \mathrm{m}}{2m_0} f_0$ in literature, which is derived from the one-term Taylor series expansion (assuming a small Δm).[55] Here, this equation is not applicable as the adsorption mass Δm is comparable with CNT mass m_0. By correlating the temperature with the initial adsorption amount, it is found that the frequency shift (for temperature over 150 K) can be well depicted by Eq. 3 (see **Supporting Information S8**). At the low temperature of 100 K, the dense adsorption layer deviates the vibrational behaviour from a simply mass-spring approximation. It is surprising to note that the resonance frequency increases remarkably in the temperature range from 100 K (122 GHz) to 250 K (140 GHz) under a full gaseous environment, about 15% increment. Such high temperature-dependent characteristics of the resonance frequency suggests that a CNT mechanical resonator can be

used as a novel thermal sensor in gaseous environment, which is beyond the reach of a traditional mechanical resonator.

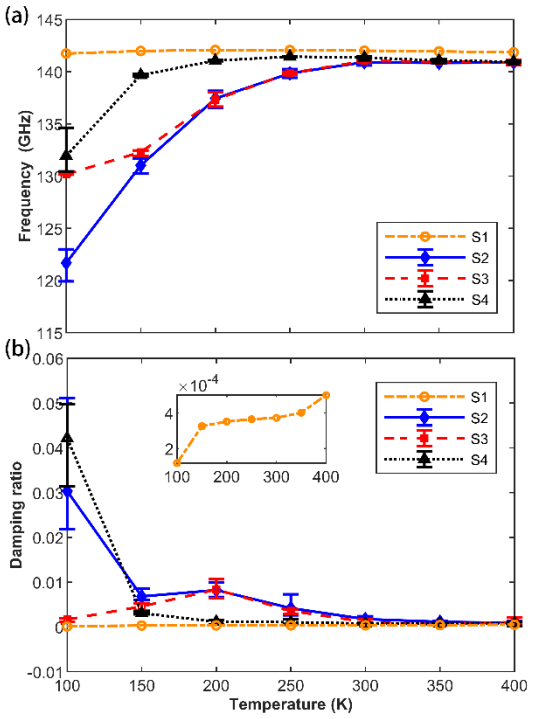

Figure 7. Influence of the temperature on the CNT resonance properties. (a) The resonance frequency as a function of temperature. (b) The damping ratio as a function of temperature.

Figure 7b illustrates the influence of the temperature on the damping ratio. For the vibration under a vacuum condition, the damping ratio increases from 1.18×10^{-4} to 5.01×10^{-4} when the temperature increases from 100 K to 400 K. For $\zeta < 0.1$, the quality factor can be calculated from $Q = 1/2\zeta$.[53] Thus, the quality factor of CNT resonator decreases from 4240 to 1000 when the temperature increases from 100 K to 400 K. The calculated quality factor is about 1340 at 300 K, much larger than that reported previously from experiments,[56] which is ascribed from the ideal simulation conditions. In consist with previous experimental and simulation results,[57-59] the quality factor decreases when the temperature increases.

For the vibration under the gaseous environment, the damping ratio is much larger, which shows an opposite decreasing tendency with the temperature (compared with the vibration under the vacuum condition, Figure 7b). For instance, the damping ratio decreases

from 0.03 at 100 K to 0.007 at 150 K. After 200 K, it decreases gradually with the temperature. To exploit the underlying mechanisms, we distinguish the damping effects from the internal and external adsorption by calculating the damping ratio for the vibration with partial adsorption (S3, S4). It is found that the damping ratio with only external adsorption decreases continuously with the temperature, which is much more significant at lower temperature regime (below 150 K). However, the damping ratio for the case with only internal adsorption increases until the temperature approaches 200 K, which is larger than the external damping ratio in the temperature range of 150 K to 250 K. The summation of these two damping ratios agrees well with the total damping ratio. Since the damping ratio with external adsorption is much larger than the internal damping at 100 K, which dominates the overall damping effect at low temperature and leads to an overall decreasing damping ratio. Similar results are observed from the vibration of others CNTs, including CNT (8, 8), CNT (12, 12), and CNT (15, 15), see **Supporting Information S9**. Theoretically, there are two kinds of collisions that will induce energy dissipation (or damping effect) during vibration: the collisions between gas molecules, and the collisions between gas molecules and the CNT surface (or carbon atoms). Due to the enclosed small space inside the CNT, the internal damping effect is expected to be enhanced (or more frequent) at higher temperature (if assuming a same amount of the trapped molecules). While, considering the decreasing adsorption amount at higher temperature but higher kinetic energy of the gas molecules, further work is required to quantify the relationship between the damping ratio and the temperature.

Before concluding, we also assess the impacts from the pressure on the vibrational properties of CNT mechanical resonators. For such purpose, we construct the adsorption models with a pressure ranging from 0.2 bar to 1.8 bar. A uniform temperature of 100 K is adopted with an excitation velocity amplitude of 1 Å/ps. As expected, the resonance frequency decreases with pressure, while the damping ratio increases with pressure (see Supporting

Information S1). Such observation is in line with the mass-spring approximation, i.e., $f = \sqrt{k/m}/2\pi$. At higher pressure, the adsorption amount (mass) is larger and thus a smaller resonance frequency is observed. Meanwhile, the increased adsorption and free gas molecules at higher pressure lead to stronger energy dissipation, which is caused by more frequent collisions among gas molecules and between gas molecules and carbon atoms.

Conclusions

By taking the doubly clamped (10,10) CNT as a representative system, this work reports a first-time in-detail investigation on the impacts of gaseous environment on the vibrational properties of the nanoscale mechanical resonators. Vibration tests reveal that the gaseous environment exerts a significant effect on the performance of the CNT mechanical resonator. The vibration amplitude (the mass centre of the CNT) experiences a sharp reduction of about 80% within a simulation time of about 100 ps. Comparing with the vacuum condition, the gaseous environment (including the free gas molecules and adsorption) is found to lower the resonance frequency and remarkably enhance the damping ratio (or suppress the quality factor). Since the N_2 molecules are attached to the CNT surfaces through weak vdW interactions, i.e., physisorption, such fact leads to a dynamic desorption and re-adsorption process during vibration. Under a relatively large excitation, three distinguishable changing stages can be identified for the total gas adsorption, including initial desorption, re-adsorption, and saturated adsorption. The desorption happens within a simulation time of ~ 50 ps, which is triggered by the sudden velocity excitation applied to the system. A large initial excitation is found to lead to smaller adsorption, and a reduced damping effect.

The increased adsorption and free gas molecules at higher pressure leads to a smaller resonance frequency and enhanced damping effect. The strong correlation between the adsorption and temperature results in a strong effect on the resonance properties from the

temperature. Specifically, the resonance frequency increases when the temperature increases. Opposite to the vibration under vacuum condition, the damping ratio decreases when the temperature increases under gaseous environment. Strikingly, the resonance frequency is found to increase remarkably in the temperature range from 100 K (122 GHz) to 250 K (140 GHz) under a full gaseous environment, about 15% increment. Such high temperature-dependent characteristics of the resonance frequency suggests that a CNT mechanical resonator can be used as a novel thermal sensor in gaseous environment that is beyond the reach of a traditional mechanical resonator. Overall, this work establishes a first-time comprehensive understanding of the impacts of the gaseous environment on the performance of CNT mechanical resonator. This study should shed lights on the applications of mechanical nano-resonators in fluid environment, such as the application in biological detection, gas sensing, chemical analysis, or atmospheric pressure sensing.

Supporting Information

The Supporting Information is available free of charge, including: pressure impacts on the frequency and damping ratio; gas adsorption at different temperatures; VACF and DOS for N_2 and CNT; RDF of N_2 adsorbates; influence from simulation settings; temperature increment of N_2 molecules; kinetic energy of N_2 molecules; temperature impacts on the resonance frequency and damping ratio.

AUTHOR INFORMATION

Corresponding Author

*E-mail: zhan.haifei@qut.edu.au; yuantong.gu@qut.edu.au

Author Contributions

Y.N. carried out the simulation. Y.N., H.Z., Z.Z, B.A., and Y.G. conducted the analysis and discussion.

Notes

The authors declare no competing financial interests.

ACKNOWLEDGEMENT

Supports from the ARC Discovery Project (DP170102861) and the High Performance Computer resources provided by the Queensland University of Technology (QUT) are gratefully acknowledged.

REFERENCE

1. Chaste, J.; Eichler, A.; Moser, J.; Ceballos, G.; Rurali, R.; Bachtold, A., A Nanomechanical Mass Sensor with Yoctogram Resolution. *Nat. Nanotechnol.* **2012**, *7*, 301.

2. Sader, J. E.; Hanay, M. S.; Neumann, A. P.; Roukes, M. L., Mass Spectrometry Using Nanomechanical Systems: Beyond the Point-Mass Approximation. *Nano Lett.* **2018**, *18*, 1608-1614.

3. Tsioutsios, I.; Tavernarakis, A.; Osmond, J.; Verlot, P.; Bachtold, A., Real-Time Measurement of Nanotube Resonator Fluctuations in an Electron Microscope. *Nano Lett.* **2017**, *17*, 1748-1755.

4. de Bonis, S. L.; Urgell, C.; Yang, W.; Samanta, C.; Noury, A.; Vergara-Cruz, J.; Dong, Q.; Jin, Y.; Bachtold, A., Ultrasensitive Displacement Noise Measurement of Carbon Nanotube Mechanical Resonators. *Nano Lett.* **2018**, *18*, 5324-5328.

5. Tavernarakis, A.; Stavrinadis, A.; Nowak, A.; Tsioutsios, I.; Bachtold, A.; Verlot, P., Optomechanics with a Hybrid Carbon Nanotube Resonator. *Nat. Commun.* **2018**, *9*, 662.

6. Dong, M.; Sahin, O., A Nanomechanical Interface to Rapid Single-Molecule Interactions. *Nat. Commun.* **2011**, *2*, 247.

7. Verbiest, G. J.; Kirchhof, J. N.; Sonntag, J.; Goldsche, M.; Khodkov, T.; Stampfer, C., Detecting Ultrasound Vibrations with Graphene Resonators. *Nano Lett.* **2018**, *18*, 5132-5137.

8. Khivrich, I.; Clerk, A. A.; Ilani, S., Nanomechanical Pump–Probe Measurements of Insulating Electronic States in a Carbon Nanotube. *Nat. Nanotechnol.* **2019**, *14*, 161-167.

9. Roy, S. K.; Sauer, V. T. K.; Westwood-Bachman, J. N.; Venkatasubramanian, A.; Hiebert, W. K., Improving Mechanical Sensor Performance through Larger Damping. *Science* **2018**, *360*, eaar5220.

10. Gieseler, J.; Novotny, L.; Quidant, R., Thermal Nonlinearities in a Nanomechanical Oscillator. *Nature Physics* **2013**, *9*, 806.

11. Barnard, A. W.; Zhang, M.; Wiederhecker, G. S.; Lipson, M.; McEuen, P. L., Real-Time Vibrations of a Carbon Nanotube. *Nature* **2019**, *566*, 89-93.

12. Niguès, A.; Siria, A.; Verlot, P., Dynamical Backaction Cooling with Free Electrons. *Nat. Commun.* **2015**, *6*, 8104.

13. Luo, G.; Zhang, Z.-Z.; Deng, G.-W.; Li, H.-O.; Cao, G.; Xiao, M.; Guo, G.-C.; Tian, L.; Guo, G.-P., Strong Indirect Coupling between Graphene-Based Mechanical Resonators via a Phonon Cavity. *Nat. Commun.* **2018**, *9*, 383.

14. Ekinci, K. L.; Yang, Y. T.; Roukes, M. L., Ultimate Limits to Inertial Mass Sensing Based Upon Nanoelectromechanical Systems. *J. Appl. Phys.* **2004**, *95*, 2682-2689.

15. Cleland, A. N.; Roukes, M. L., Noise Processes in Nanomechanical Resonators. *J. Appl. Phys.* **2002**, *92*, 2758-2769.

16. Kim, S. Y.; Park, H. S., The Importance of Edge Effects on the Intrinsic Loss Mechanisms of Graphene Nanoresonators. *Nano Lett.* **2009**, *9*, 969-974.

17. Tsaturyan, Y.; Barg, A.; Polzik, E. S.; Schliesser, A., Ultracoherent Nanomechanical Resonators via Soft Clamping and Dissipation Dilution. *Nat. Nanotechnol.* **2017**, *12*, 776.

18. Tao, Y.; Boss, J. M.; Moores, B. A.; Degen, C. L., Single-Crystal Diamond Nanomechanical Resonators with Quality Factors Exceeding One Million. *Nat. Commun.* **2014**, *5*, 3638.

19. Moser, J.; Eichler, A.; Güttinger, J.; Dykman, M. I.; Bachtold, A., Nanotube Mechanical Resonators with Quality Factors of up to 5 Million. *Nat. Nanotechnol.* **2014**, *9*, 1007.

20. Calleja, M.; Kosaka, P. M.; San Paulo, A.; Tamayo, J., Challenges for Nanomechanical Sensors in Biological Detection. *Nanoscale* **2012**, *4*, 4925-38.

21. Kara, V.; Sohn, Y. I.; Atikian, H.; Yakhot, V.; Lončar, M.; Ekinci, K. L., Nanofluidics of Single-Crystal Diamond Nanomechanical Resonators. *Nano Lett.* **2015**, *15*, 8070-8076.

22. Hanay, M. S.; Kelber, S.; Naik, A. K.; Chi, D.; Hentz, S.; Bullard, E. C.; Colinet, E.; Duraffourg, L.; Roukes, M. L., Single-Protein Nanomechanical Mass Spectrometry in Real Time. *Nat Nanotechnol* **2012**, *7*, 602-8.

23. Fanget, S.; Hentz, S.; Puget, P.; Arcamone, J.; Matheron, M.; Colinet, E.; Andreucci, P.; Duraffourg, L.; Myers, E.; Roukes, M. L., Gas Sensors Based on Gravimetric Detection—a Review. *Sensors and Actuators B: Chemical* **2011**, *160*, 804-821.

24. Li, M.; Myers, E. B.; Tang, H. X.; Aldridge, S. J.; McCaig, H. C.; Whiting, J. J.; Simonson, R. J.; Lewis, N. S.; Roukes, M. L., Nanoelectromechanical Resonator Arrays for Ultrafast, Gas-Phase Chromatographic Chemical Analysis. *Nano Lett.* **2010**, *10*, 3899-3903.

25. Bargatin, I.; Myers, E. B.; Aldridge, J. S.; Marcoux, C.; Brianceau, P.; Duraffourg, L.; Colinet, E.; Hentz, S.; Andreucci, P.; Roukes, M. L., Large-Scale Integration of Nanoelectromechanical Systems for Gas Sensing Applications. *Nano Lett.* **2012**, *12*, 1269-74.

26. Henriksson, J.; Villanueva, L. G.; Brugger, J., Ultra-Low Power Hydrogen Sensing Based on a Palladium-Coated Nanomechanical Beam Resonator. *Nanoscale* **2012**, *4*, 5059-64.

27. McCaig, H. C.; Myers, E.; Lewis, N. S.; Roukes, M. L., Vapor Sensing Characteristics of Nanoelectromechanical Chemical Sensors Functionalized Using Surface-Initiated Polymerization. *Nano Lett.* **2014**, *14*, 3728-32.

28. Venstra, W. J.; Capener, M. J.; Elliott, S. R., Nanomechanical Gas Sensing with Nonlinear Resonant Cantilevers. *Nanotechnology* **2014**, *25*, 425501.

29. Kumar, M.; Bhaskaran, H., Ultrasensitive Room-Temperature Piezoresistive Transduction in Graphene-Based Nanoelectromechanical Systems. *Nano Lett.* **2015**, *15*, 2562-2567.

30. Sazonova, V.; Yaish, Y.; Üstünel, H.; Roundy, D.; Arias, T. A.; McEuen, P. L., A Tunable Carbon Nanotube Electromechanical Oscillator. *Nature* **2004**, *431*, 284-287.

31. Zhang, W.; Turner, K., Frequency Dependent Fluid Damping of Micro/Nano Flexural Resonators: Experiment, Model and Analysis. *Sensors and Actuators, A: Physical* **2007**, *134*, 594-599.

32. Van Eysden, C. A.; Sader, J. E., Frequency Response of Cantilever Beams Immersed in Compressible Fluids with Applications to the Atomic Force Microscope. *J. Appl. Phys.* **2009**, *106*.

33. Zhang, C.; Jiao, Y.; Ma, F.; Kasi Matta, S.; Bottle, S.; Du, A., Free-Radical Gases on Two-Dimensional Transition-Metal Disulfides (XS_2, X = Mo/W): Robust Half-Metallicity for Efficient Nitrogen Oxide Sensors. *Beilstein Journal of Nanotechnology* **2018**, *9*, 1641-1646.

34. Skoulidas, A. I.; Sholl, D. S.; Johnson, J. K., Adsorption and Diffusion of Carbon Dioxide and Nitrogen through Single-Walled Carbon Nanotube Membranes. *J. Chem. Phys.* **2006**, *124*.

35. Arora, G.; Wagner, N. J.; Sandler, S. I., Adsorption and Diffusion of Molecular Nitrogen in Single Wall Carbon Nanotubes. *Langmuir : the ACS journal of surfaces and colloids* **2004**, *20*, 6268-6277.

36. Zhao, J.; Buldum, A.; Han, J.; Lu, J. P., Gas Molecule Adsorption in Carbon Nanotubes and Nanotube Bundles. *Nanotechnology* **2002**, *13*, 195-200.

37. Maddox, M. W.; Gubbins, K. E., Molecular Simulation of Fluid Adsorption in Buckytubes. *Langmuir* **1995**, *1995*, 3988-3996.

38. Agnihotri, S.; Mota, J. P. B.; Rostam-Abadi, M.; Rood, M. J., Adsorption Site Analysis of Impurity Embedded Single-Walled Carbon Nanotube Bundles. *Carbon* **2006**, *44*, 2376-2383.

39. Fujiwara, A.; Ishii, K.; Suematsu, H.; Kataura, H.; Maniwa, Y.; Suzuki, S.; Achiba, Y., Gas Adsorption in the inside and Outside of Single-Walled Carbon Nanotubes. *Chem. Phys. Lett.* **2001**, *336*, 205-211.

40. Stuart, S. J.; Tutein, A. B.; Harrison, J. A., A Reactive Potential for Hydrocarbons with Intermolecular Interactions. *The Journal of Chemical Physics* **2000**, *112*, 6472-6486.

41. Plimpton, S., Fast Parallel Algorithms for Short-Range Molecular Dynamics. *Journal of Computational Physics* **1995**, *117*, 1-19.

42. Evans, D. J.; Holian, B. L., The Nose–Hoover Thermostat. *The Journal of Chemical Physics* **1985**, *83*, 4069-4074.

43. Zhan, H. F.; Gu, Y. T., Surface Effects on the Dual-Mode Vibration of ⟨1 1 0⟩ Silver Nanowires with Different Cross-Sections. *J. Phys. D: Appl. Phys.* **2012**, *45*, 465304.

44. Zhan, H. F.; Gu, Y. T., A Fundamental Numerical and Theoretical Study for the Vibrational Properties of Nanowires. *J. Appl. Phys.* **2012**, *111*, 124303-9.

45. Zhan, H. F.; Gu, Y. T.; Park, H. S., Beat Phenomena in Metal Nanowires, and Their Implications for Resonance-Based Elastic Property Measurements. *Nanoscale* **2012**, *4*, 6779-6785.

46. Talapatra, S.; Zambano, A. Z.; Weber, S. E.; Migone, A. D., Gases Do Not Adsorb on the Interstitial Channels of Closed-Ended Single-Walled Carbon Nanotube Bundles. *Phys. Rev. Lett.* **2000**, *85*.

47. Vallabhaneni, A. K.; Rhoads, J. F.; Murthy, J. Y.; Ruan, X., Observation of Nonclassical Scaling Laws in the Quality Factors of Cantilevered Carbon Nanotube Resonators. *J. Appl. Phys.* **2011**, *110*.

48. Treacy, M. M. J.; Ebbesen, T. W.; Gibson, J. M., Exceptionally High Young's Modulus Observed for Individual Carbon Nanotubes. *Nature* **1996**, *381*, 678-680.

49. Sansa, M.; Sage, E.; Bullard, E. C.; Gély, M.; Alava, T.; Colinet, E.; Naik, A. K.; Villanueva, L. G.; Duraffourg, L.; Roukes, M. L., et al., Frequency Fluctuations in Silicon Nanoresonators. *Nature Nanotechnology* **2016**, *11*, 552-558.

50. Robins, W. P., *Phase Noise in Signal Sources : (Theory and Applications)*; Peregrinus on behalf of the Institution of Electrical Engineers: London, 1982.

51. Djuri, Z.; Jakši, O.; Randjelovi, D., Adsorption-Desorption Noise in Micromechanical Resonant Structures. *Sensors and Actuators, A: Physical* **2002**, *96*, 244-251.

52. Cleland, A. N.; Roukes, M. L., Noise Processes in Nanomechanical Resonators. *J. Appl. Phys.* **2002**, *92*, 2758-2769.

53. De Silva, C. W., *Vibration Damping, Control, and Design*, 1st ed. ed.; Chapman and Hall/CRC: Baton Rouge, 2007.

54. Zhan, H. F.; Gu, Y. T., Modified Beam Theories for Bending Properties of Nanowires Considering Surface/Intrinsic Effects and Axial Extension Effect. *J. Appl. Phys.* **2012**, *111*.

55. Jensen, K.; Kim, K.; Zettl, A., An Atomic-Resolution Nanomechanical Mass Sensor. *Nat. Nanotechnol.* **2008**, *3*, 533.

56. Lassagne, B.; Garcia-Sanchez, D.; Aguasca, A.; Bachtold, A., Ultrasensitive Mass Sensing with a Nanotube Electromechanical Resonator. *Nano Lett.* **2008**, *8*, 3735-3738.

57. Huttel, A. K.; Steele, G. A.; Witkamp, B.; Poot, M.; Kouwenhoven, L. P.; Van Der Zant, H. S. J., Carbon Nanotubes as Ultrahigh Quality Factor Mechanical Resonators. *Nano Lett.* **2009**, *9*, 2547-2552.

58. Jiang, H.; Yu, M. F.; Liu, B.; Huang, Y., Intrinsic Energy Loss Mechanisms in a Cantilevered Carbon Nanotube Beam Oscillator. *Phys. Rev. Lett.* **2004**, *93*, 1-4.

59. Zolfagharkhani, G.; Gaidarzhy, A.; Shim, S. B.; Badzey, R. L.; Mohanty, P., Quantum Friction in Nanomechanical Oscillators at Millikelvin Temperatures. *Physical Review B - Condensed Matter and Materials Physics* **2005**, *72*, 1-5.

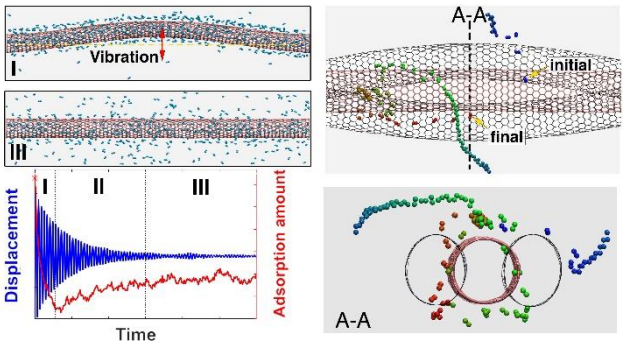

TOC Graphic